



Article

Diastereoselective Synthesis of Novel Spiro-Phosphacoumarins and Evaluation of Their Anti-Cancer Activity

Valeriia V. Sennikova ¹, Alena V. Zalaltdinova ¹ , Yulia M. Sadykova ¹ , Ayrat R. Khamatgalimov ^{1,*} , Almir S. Gazizov ^{1,*} , Alexandra D. Voloshina ¹ , Anna P. Lyubina ¹, Syumbelya K. Amerhanova ¹, Julia K. Voronina ² , Elena A. Chugunova ¹ , Nurbol O. Appazov ³ , Alexander R. Burilov ¹ and Michail A. Pudovik ¹

- ¹ Arbuzov Institute of Organic and Physical Chemistry, FRC Kazan Scientific Center, Russian Academy of Sciences, Arbuzova str. 8, 420088 Kazan, Russia
² N.S. Kurnakov Institute of General and Inorganic Chemistry, Russian Academy of Sciences, Leninsky Ave. 31, 119991 Moscow, Russia
³ Korkyt Ata Kyzylorda State University, 29A Aiteke Bi St., Kyzylorda 120014, Kazakhstan
* Correspondence: ayrat_kh@iopc.ru (A.R.K.); agazizov@iopc.ru (A.S.G.)

Abstract: Herein we present the regio- and diastereoselective synthesis of novel pyrrolidine-fused spiro-dihydrophosphacoumarins via intermolecular [3 + 2] cycloaddition reaction. The presented approach is complementary to existing ones and provides an easy entry to the otherwise inaccessible derivatives. Additionally, the unprecedented pathway of the reaction of 4-hydroxycoumarin with azomethine ylides is described. The anti-cancer activity of the obtained compounds was tested in vitro, the most potent compound being 2.6-fold more active against the HuTu 80 cell line than the reference 5-fluorouracil, with a selectivity index > 32.

Keywords: phosphacoumarin; azomethine ylide; cycloaddition; anti-cancer; cytotoxicity; quantum chemistry



Citation: Sennikova, V.V.; Zalaltdinova, A.V.; Sadykova, Y.M.; Khamatgalimov, A.R.; Gazizov, A.S.; Voloshina, A.D.; Lyubina, A.P.; Amerhanova, S.K.; Voronina, J.K.; Chugunova, E.A.; et al.

Diastereoselective Synthesis of Novel Spiro-Phosphacoumarins and Evaluation of Their Anti-Cancer Activity. *Int. J. Mol. Sci.* **2022**, *23*, 14348. <https://doi.org/10.3390/ijms232214348>

Academic Editor: Dmitry Aminin

Received: 27 October 2022

Accepted: 15 November 2022

Published: 18 November 2022

Publisher's Note: MDPI stays neutral with regard to jurisdictional claims in published maps and institutional affiliations.



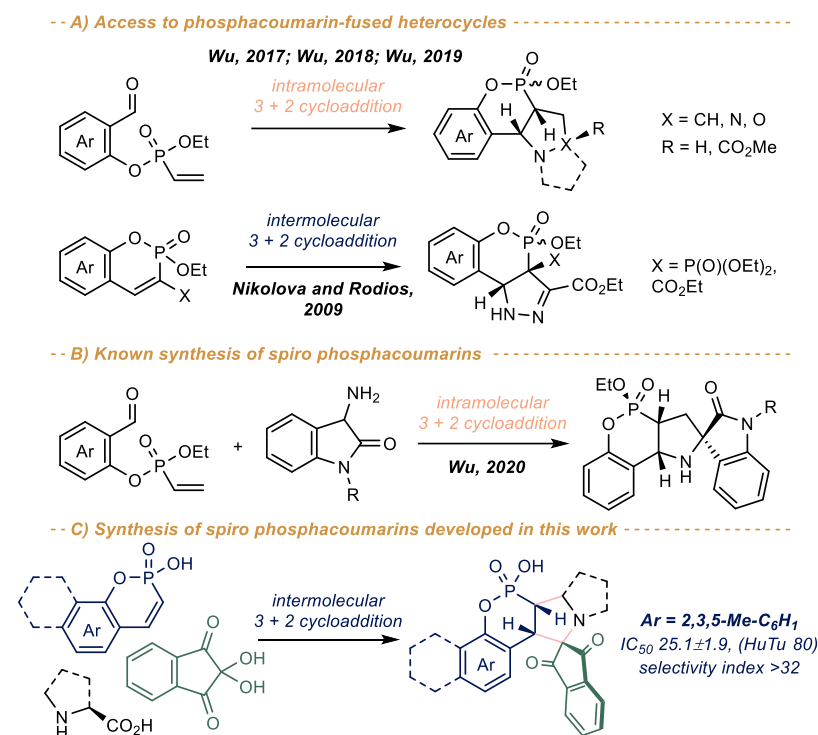
Copyright: © 2022 by the authors. Licensee MDPI, Basel, Switzerland. This article is an open access article distributed under the terms and conditions of the Creative Commons Attribution (CC BY) license (<https://creativecommons.org/licenses/by/4.0/>).

1. Introduction

Coumarins and dihydrocoumarins are ubiquitous in nature and have attracted considerable attention due to their biological properties [1–3]. Among known activities of coumarins, their anti-cancer properties [4,5] have gained an increasing interest and represent an emerging area of research, as indicated by recent reviews [6,7]. A number of substituted coumarins have been synthesized and tested in attempts to enhance their activity and pharmacological properties. The phosphorus-containing analogues of coumarins, the phosphacoumarins, have recently appealed as promising compounds possessing interesting structural, chemical and biological properties [8,9]. Various approaches to these compounds exist [8,10–12], which have been summarized in a recent review paper [13]. Despite the ongoing research in this field, the synthesis of heterocycle annelated and spiro derivatives of phosphacoumarins and dihydrophosphacoumarins is still scarce (see [14] for the review).

The approach to the pyrazolidin-3-on-, pyrrolidine- and isoxazolidine-fused phosphacoumarins via intramolecular 1,3-dipolar cycloaddition of salicylaldehyde-derived vinylphosphonates has been developed by Wu and coworkers (Scheme 1A) [15–17]. Earlier, Nikolova and Rodios reported the synthesis of pyrazole-fused phosphacoumarins using intermolecular [3 + 2] cycloaddition of phosphacoumarins with ethyl diazoacetate [18]. The only synthesis of oxindole spiro phosphacoumarins has been described by Wu [19], which also involved the intramolecular [3 + 2] cycloaddition of vinylphosphonates (Scheme 1B). This is in sharp contrast to parent coumarins, for which a number of spiro derivatives are known [20,21], including rather complex polycyclic [22] and even fullerene-fused ones [23].

As a result of our ongoing research in this area [24–26], herein we report a highly diastereoselective synthesis of spiro dihydrophosphacoumarins via intramolecular [3 + 2] cycloaddition of phosphacoumarins with some azomethine ylides (Scheme 1C). The proposed approach is complementary to that reported by Wu [19] and provides an easy entry to the novel pyrrolidine-fused spiro-phosphacoumarins derivatives, which are inaccessible via Wu’s method. The mechanism of the reaction and its regio- and diastereoselectivity was explored using quantum chemistry calculations. The cytotoxicity of the obtained compounds towards normal and cancer cell lines was also tested, the most potent compound being 3-fold more active than reference 5-fluorouracil and exhibiting a selectivity index > 32.

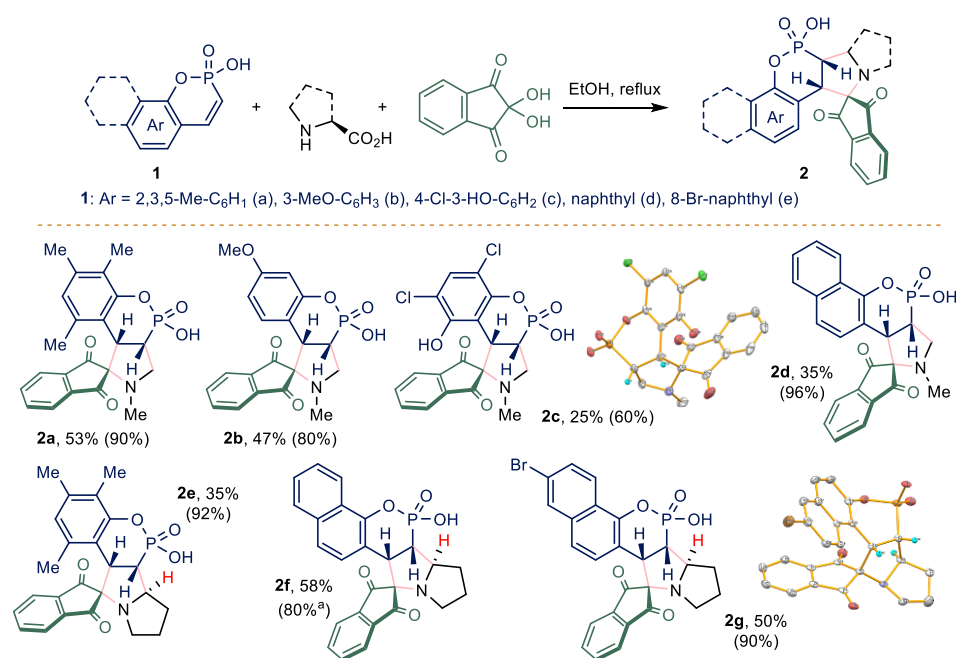


Scheme 1. Synthesis of heterocycle-fused phosphacoumarins via [3 + 2] cycloaddition reactions [15–18] (A), the only reported synthesis of spiro phosphacoumarins [19] (B) and the complementary approach developed in this work (C).

2. Results and Discussion

2.1. Chemistry

We started our research with the optimization of reaction conditions using phosphacoumarin **1a**, ninhydrin and sarcosine as model compounds. Pleasingly, simple refluxing of reactants in ethanol provided the target compound **2a** with a *ca* 90% yield according to ³¹P NMR data (Scheme 2). Additionally, the reaction proceeded in a highly regio- and diastereoselective manner (*dr* > 95: 5), which was also evidenced by ³¹P NMR data. We succeeded in the isolation of the single diastereomer from the reaction mixture with a 53% yield. Convinced of the possibility of the formation of the desired spiro dihydrophosphacoumarins, we further extended the reaction scope using phosphacoumarins **1b–e**. The reaction proceeded smoothly, providing target spiro compounds with a 60–96% yield according to NMR data. However, isolated yields were considerably lower due to the degradation of phosphacoumarins **2** during silica gel column purification, leading to the formation of highly polar compounds. Unfortunately, we were not able to isolate and identify these byproducts.



Scheme 2. Synthesis of spiro pyrrolidinophosphacoumarins **2**. Isolated yield is given, yield according to ³¹P NMR is given in parenthesis. ^a Isolated as a mixture of diastereomers with *dr* 12: 1 (see discussion in the text).

Presumably, the electron-donating groups in aromatic moiety promote the reaction, whereas electron withdrawing chlorine substituent clearly lowers the yield of the compound **2c**. In all cases, the target compounds were formed as single regioisomers with an excellent diastereoselectivity (*dr* > 95: 5). The configuration of the compound **2c** was determined to be *SS/RR* with X-ray analysis.

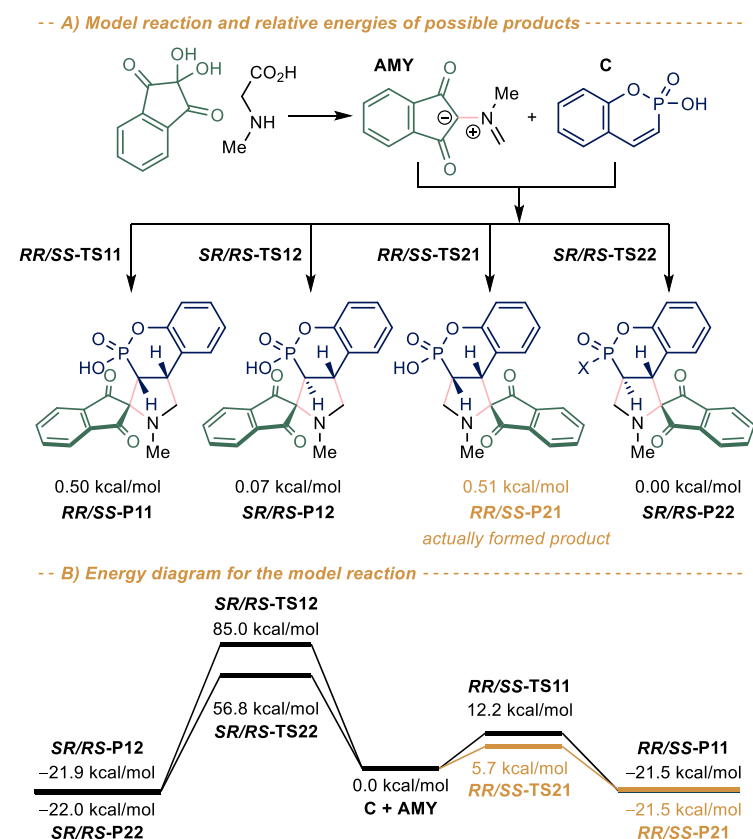
We also tested *L*-proline as an amino acid component in this reaction, which also furnished tetracyclic spiro phosphacoumarins **2e–g**. Despite one more stereocenter being present in these cases, the diastereoselectivity of the reaction remained fairly high (*dr* > 95: 5 according to ³¹P NMR data). Fortunately, we were able to grow crystals which were suitable for x-ray analysis of the compound **2g**, which allowed us to assign *SRS/RSR* configuration to the obtained diastereomers.

Despite the ³¹P NMR data of the reaction mixtures in all cases indicating the presence of single desired product, the compound **2f** was isolated as a mixture of diastereomers (*dr* 12: 1, see Supporting Information, Figure S31). This may be explained by the relatively low sensitivity of the ³¹P NMR method, not allowing the detection of very low concentrations (*ca* 2–3%) of the second diastereomer in the reaction mixtures. However, the reaction mixture could be enriched with this unobservable diastereomer during work-up, which is presumably the case for the compound **2f**.

2.2. Quantum Chemistry Studies

In order to gain more insight into the regio- and diastereoselectivity of the reaction of phosphacoumarins with azomethine ylides, quantum chemistry studies were carried out using unsubstituted phosphacoumarin **C** as the model compound (Scheme 3A). The first stage of the reaction, i.e., the formation of azomethine ylide **AMY** from ninhydrin and sarcosine, is a well-known process (see, e.g., [27,28]) and therefore was not modelled. The second stage is the [3 + 2] dipolar cycloaddition of intermediate **AMY** and compound **C**. In principle, two regioisomeric products may be formed at this stage. Since each one can exist as two diastereomers, this gives four possible final products in total. So, to identify the most preferred regioisomer of the reaction, the quantum chemistry calculations of the reagents **C** and **AMY**, the products **P** as well as the corresponding transition states **TS** were performed. Analysis of quantum chemical results shows that for the charged

species taking solvation model with a protic ethanol solvent into account play a crucial role in stabilizing the intermediates and products of [3 + 2]-cycloaddition (see Table S2 in Supporting Information).



Scheme 3. (A) Model [3 + 2] cycloaddition of phosphacoumarin C with ninhydrin-derived azomethine ylide AMY alongside relative energies of the possible isomeric products (ΔE , kcal/mol); (B) Energy diagram (ΔE , kcal/mol) as obtained from quantum chemistry calculations (PW6B95D/def2-TZVPD//B3LYP/6-31 + G*, Gaussian16). The sum of the total energies of reactants (C + AMY) is taken as zero.

According to the obtained quantum chemistry data, the reaction under study is exothermic (thermal effects are 21.5–22.0 kcal/mol for all expected reaction pathways) with the compound *SR/RS-P22* being slightly lower in energy compared to all the others (Scheme 3A, see also Supporting Information, Table S1). This is somewhat counterintuitive, since one would expect isomers *RR/SS-P21* and *SR/RS-P22* to be much more unfavourable due to sterical hindrance caused by the ninhydrin moiety. However, the energy difference appeared to be *ca* 0.1–0.5 kcal/mol only. Obviously, the preferable formation of the *RR/SS-P21* isomer cannot be attributed to its thermodynamic stability.

On the other hand, the calculated transition state energies differ significantly for all products (Scheme 3B, see also Supporting Information, Table S2). The transition state energies for the *SR/RS*-diastereomers are significantly higher than for their *SS/RR*-counterparts for both regioisomers. Taking into account the energy difference (*ca* 51–73 kcal/mol), the barriers can be considered prohibitively high for the *SR/RS*-diastereomers formation. On the other hand, the barrier for the formation of the *SS/RR-P21* diastereomer is *ca* 7 kcal/mol lower compared to that of the *SS/RR-P11*-diastereomer. According to the Arrhenius equation, 1 kcal/mol difference in activation energies results in more than a 6-fold difference in reaction rates at room temperature. Thus, the formation of the compound *SS/RR-P21* is much more preferable. These results are in complete agreement with the experimental observations. Thus, the high regio- and diastereoselectivity of the reaction

may be attributed to the faster formation of the *SS/RR-P21*-isomer, which appears to be a product of a kinetic control.

2.3. Biological Studies

2.3.1. In Vitro Cytotoxicity

Next, the obtained compounds were tested for cytotoxicity against normal and cancer human cell lines at concentrations of 1–100 μM . The compounds **2f** and **2g** were excluded from these studies, however, due to their extremely low solubility in water. As seen from Table 1, all of the tested compounds exhibit low cytotoxicity against MCF-7 cancer cell line, whereas the cytotoxicity against M-HeLa cells is comparable to that of the reference compound 5-fluorouracil. Notably, some of the compounds appeared to be non-toxic to normal cells in the studies' concentrations range. Similarly, the cytotoxicity of the obtained compounds against HuTu 80 cancer cells is either lower or comparable to the cytotoxicity of 5-fluorouracil.

Table 1. Cytotoxic effects of phosphacoumarins **2** on the cancer and normal human cell lines ¹.

Cmpd	Cancer Cell Line						Normal Cell Line
	M-HeLa		MCF-7		HuTu 80		Chang Liver
	IC ₅₀ , μM	SI	IC ₅₀ , μM	SI	IC ₅₀ , μM	SI	IC ₅₀ , μM
2a	52.6 \pm 4.1	>15	82.3 \pm 7.5	>10	25.1 \pm 1.9	>32	>800
2b	59.7 \pm 4.6	1	>100	ns	53.4 \pm 4.2	1.2	62.0 \pm 5.5
2c	>100	ns	77.6 \pm 6.2	ns	100 \pm 8.4	ns	>100
2d	60 \pm 5.4	ns	92.2 \pm 8.3	ns	82.6 \pm 7.6	ns	57.0 \pm 4.3
2e	>100	ns	>100	ns	>100	ns	>100
5-fluorouracil	62.0 \pm 4.7	1.4	16.7 \pm 1.3	5	65.2 \pm 5.6	1.3	86.3 \pm 6.5

¹ Three independent experiments were carried out; "ns" means no selectivity.

The remarkable exception is the phosphacoumarin **2a**. Its cytotoxicity against HuTu 80 cell line is *ca* 2.6-fold higher than the cytotoxicity of the reference compound, whereas the cytotoxicity against the Chang liver normal cell line is more than 10-fold lower, which gives a selectivity index > 32. For the M-HeLa cells, the cytotoxicity of compound **2a** was somewhat higher than that of the reference compound (52.6 \pm 4.1 vs. 62.0 \pm 4.7), with a selectivity index > 15. Finally, although the activity against MCF-7 cell line was considerably lower compared to the 5-fluorouracil, the selectivity index still remained above 10. Since compounds with a selectivity index > 10 are considered highly selective [29], the phosphacoumarin **2a** is a promising lead for further studies.

2.3.2. Cell Cycle Analysis

Taking into account the high potency and selectivity of the compound **2a**, some additional experiments were carried out to study in more details its anti-cancer action. The mechanism of action of cytotoxic agents is often associated with cell cycle arrest, which leads to a slowing down of cell proliferation. So, we have performed a cell cycle analysis for the HuTu 80 cells using flow cytometry. According to the obtained data, the presence of compound **2a** at concentrations of IC₅₀/2 (12.5 μM) and IC₅₀ (25 μM) after 24 h leads to an increase in the number of cells in the G1/G0 phase up to 79.0% and 81.0%, respectively, compared with the control of 77% (Figure 1). Meanwhile, the proportion of cells in S phase decreased almost by half (8.2% vs. 4.7%). Taken together, these results indicate that the compound **2a** treatment induces G0/G1 phase arrest and reduces the S phase of the cell cycle, leading to an inhibition in the proliferation of HuTu 80 cells.

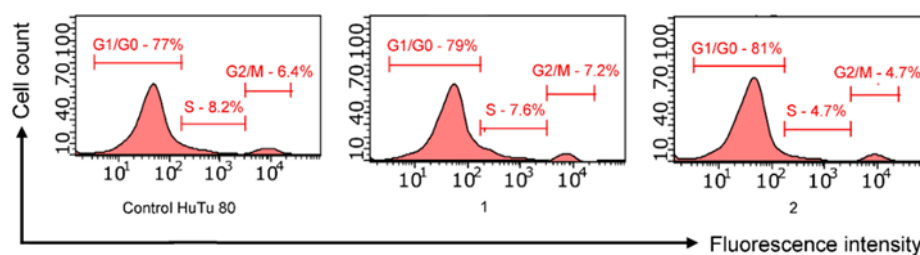


Figure 1. Effect of compound **2a** on cell cycle of HuTu 80 by flow cytometry. 1–**2a** at $IC_{50}/2$ concentration (12.5 μ M); 2–**2a** at IC_{50} concentration (25 μ M).

2.3.3. Induction of Apoptotic Effects

Apoptosis is one of the most important mechanisms used to screen for new anticancer agents. The ability of the lead compound **2a** to induce apoptosis in HuTu 80 cells was determined by flow cytometry using annexin V-Alexa Fluor 647. Cells were incubated in the presence of **2a** at concentrations of $IC_{50}/2$ and IC_{50} (Figure 2). It can be seen that after a 24-h incubation, the test compound begins to induce apoptosis in HuTu 80 cells. The most active apoptotic effects are manifested at an $IC_{50}/2$ concentration (12.5 μ M) in the early apoptosis stage (Figure 3).

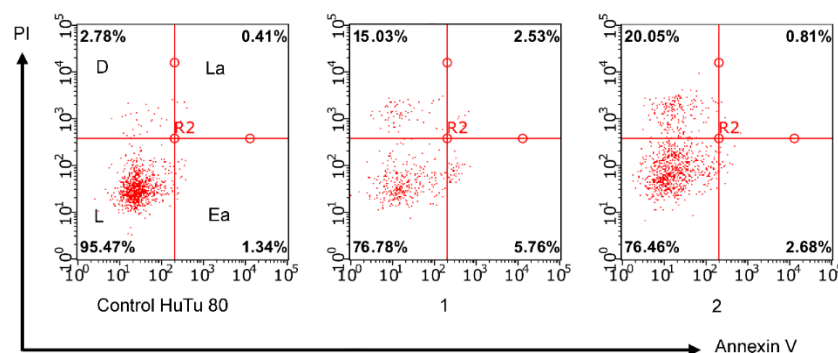


Figure 2. Apoptotic effects of compounds **2a** on HuTu 80 cells. 1–**2a** at $IC_{50}/2$ concentration (12.5 μ M); 2–**2a** at IC_{50} concentration (25 μ M).

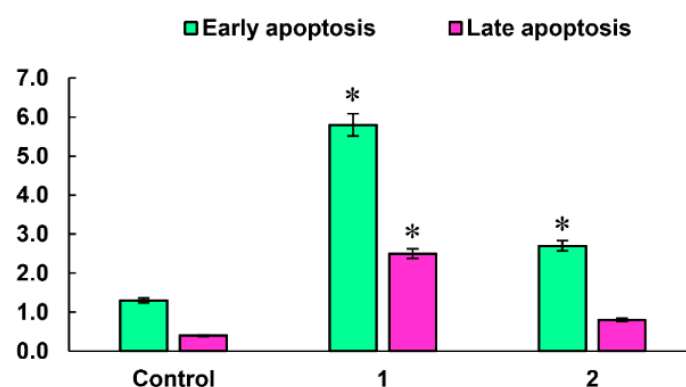


Figure 3. Representative histograms for the numbers of cells (% of total) in the early and late stages of apoptosis for the control and experimental groups. 1–**2a** at $IC_{50}/2$ concentration (12.5 μ M); 2–**2a** at IC_{50} concentration (25 μ M). The values are presented as the mean \pm SD; (*) $p < 0.05$ compared to control.

2.3.4. Mitochondrial Membrane Potential

The possibility of apoptosis through the mitochondrial pathway was assessed by flow cytometry using the JC-10 fluorescent dye (in the Mitochondria Membrane Potential Kit). In normal cells with a high membrane potential, JC-10 accumulates in the mitochondrial

matrix, where it forms aggregates with a red fluorescence. However, in apoptotic cells, a decrease in the membrane potential occurs. JC-10 diffuses from mitochondria and turns into a monomeric form, emitting a green fluorescence, which is recorded by a flow cytometer (Figure 4). After treatment with lead compound **2a** at concentrations of $IC_{50}/2$ and IC_{50} , the intensity of the green fluorescence significantly increased compared to the control (Figure 5). The results obtained indicated a significant decrease in the mitochondrial membrane potential of HuTu 80 cells. As in the experiment with V-Alexa Fluor 647, the cytotoxic effect of compound **2a** was more pronounced at $IC_{50}/2$ concentration. The results described above suggest that the mechanism of action of the leader of compound **2a** can be associated with the induction of apoptosis proceeding via the mitochondrial pathway.

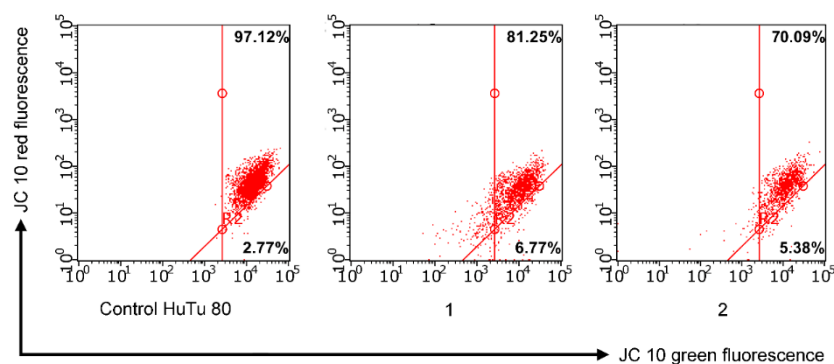


Figure 4. Flow cytometry analysis of HuTu 80 cells treated with compound **2a**. 1–**2a** at $IC_{50}/2$ concentration (12.5 μ M); 2–**2a** at IC_{50} concentration (25 μ M).

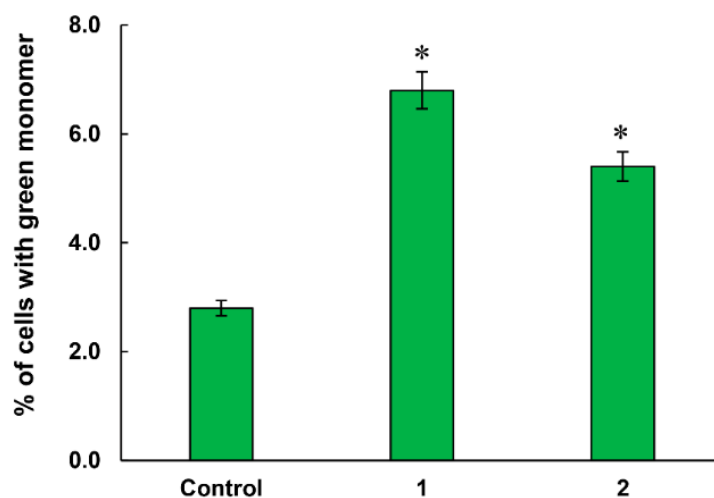


Figure 5. Quantitative determination of % cells with green monomers; 1–**2a** at $IC_{50}/2$ concentration (12.5 μ M); 2–**2a** at IC_{50} concentration (25 μ M). Values are presented as mean \pm SD; (*) $p < 0.05$ compared to control.

An increase in the production of reactive oxygen species (ROS) by compounds also characterizes the development of apoptosis along the mitochondrial pathway. Mitochondria are a potential source and target of ROS. ROS leads to dysfunction of the mitochondria and, consequently, to irreversible cell damage. In this regard, the effect of the lead compound **2a** in HuTu 80 cells on ROS production was investigated using a flow cytometry assay and the CellROX[®] Deep Red flow cytometry kit. The data presented in Figure 6 show a significant increase in CellROX[®] Deep Red fluorescence intensity dominated by $IC_{50}/2$. This indicates an increase in ROS production in the presence of compound **2a**.

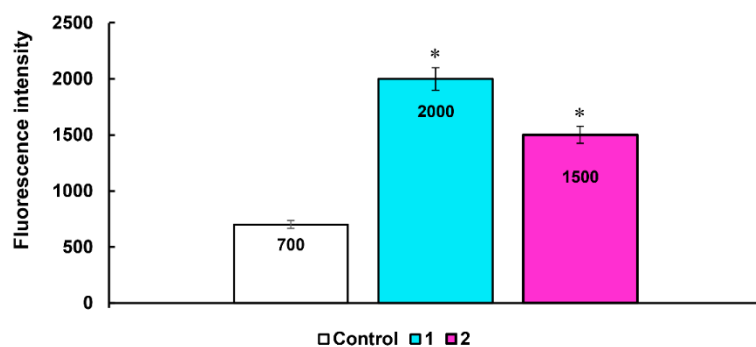


Figure 6. Induction of ROS production by lead compound **2a**. **1–2a** at concentration $IC_{50}/2$ (12.5 μ M); **2–2a** at concentration IC_{50} (25 μ M); (*) $p < 0.05$ compared to control.

3. Materials and Methods

3.1. Quantum Chemistry Calculations

All calculations were performed with Becke's three parameter hybrid exchange functional [30] and the gradient-corrected nonlocal correlation functional of Lee et al. [31] (B3LYP) in combination with the standard 6–31 + G* basis set [32–34] in the Gaussian16 package [35]. All geometry optimizations were performed without symmetry constraints (see Supporting Information, Table S3 for optimized cartesian coordinates). Since the method and the basis set used are known to have many limitations [36], geometry optimization was followed by a single-point calculation with PW6B95D functional [37] and def2-TZVPD basis set [38] to improve energies. Additionally, the Polarizable Continuum Model with the CPCM polarizable conductor calculation model was used in single-point calculations as a solvation model with the molecule of interest inside a cavity in a continuous, homogenous dielectric medium. Ethanol was used as a solvent in the used solvation model.

To ensure the calculated geometries correspond to true minima, vibrational analyses were performed using the same level of theory and the structure was accepted only if all eigenvalues of the Hessian matrix were positive. The transition states were confirmed by the presence of one negative eigenvalue in the Hessian matrix of the second derivatives. Additionally, the intrinsic reaction coordinate (IRC) was traced to ensure the transition state really connects the species involved in the reaction. The energy diagram was created with the aid of the Energy Diagram Plotter (CDXML) program [39].

3.2. Chemistry

3.2.1. General Methods

IR spectra were recorded on a UR-20 spectrometer in a 400–3600 cm^{-1} range in KBr. 1H NMR spectra were recorded on a Bruker MSL 400 spectrometer (399.93 MHz) with respect to the signals of residual protons in the deuterated solvent ($CDCl_3$, DMSO- d_6 , D_2O , CF_3COOD). The ^{13}C NMR spectra were recorded on a Bruker Avance 600 (151 MHz) spectrometer relative to the signals of residual protons from the deuterated solvent ($CDCl_3$, DMSO- d_6 , D_2O , CF_3COOD) (see Supporting information, Figures S3–S30, S32–S36 for the copies of NMR spectra). The ^{31}P NMR spectra were recorded on a Bruker Avance 600 (151 MHz) spectrometer. Elemental analysis was performed on a Carlo Erba device EA 1108. The melting points were determined in glass capillaries on a Stuart SMP 10 instrument.

The X-ray diffraction data for the crystals were collected on a Bruker D8 Venture diffractometer equipped with a CCD detector (Mo- $K\alpha$, $\lambda = 0.71073 \text{ \AA}$, graphite monochromator). Semi-empirical absorption correction was applied by the SADABS program [40]. The structures were solved by direct methods and refined by the full-matrix least squares in the anisotropic approximation for non-hydrogen atoms. The calculations were carried out by the SHELX-2014 program package [41] using Olex2 1.2 [42]. Crystallographic data for the structures reported in this paper have been deposited with the Cambridge Crystallographic Data Center (CCDC 2179367, 2179368, see Supporting information, Tables S4

and S5 and Figures S1 and S2 for the detailed data). Starting phosphacoumarins **1** were obtained by reported procedures [43].

3.2.2. General Procedure for the Synthesis of Compounds **2**

To a refluxing solution of phosphacoumarin **1** (1.8 mmol) in ethanol (5 mL), a mixture of ninhydrin (0.32 g, 1.8 mmol) and appropriate aminoacid (1.8 mmol) was added in one portion. The reaction mixture was refluxed until full consumption of starting materials (^{31}P NMR control, *ca* 12 h). The target compounds **2** were isolated in a pure form in two ways. In case of compounds **2a–d** the solvent was removed in a vacuum and the residue was purified by gradient-elution column chromatography using DCM: ethanol as eluent. In the case of compounds **2e–g**, the precipitate formed was filtered off, washed thoroughly with distilled water and dried in vacuum.

(3aS,9bS)-4-hydroxy-2,6,7,9-tetramethyl-2,3,3a,9b-tetrahydrospiro[benzo [5,6][1,2]oxaphosphinino [3,4-c]pyrrole-1,2'-indene]-1',3'-dione 4-oxide (2a)

Yield 0.25 g (53%), yellow solid, m.p. > 300 °C. IR (ν , cm^{-1}): 1080 (C-O), 1232 (P = O), 1460 (CH_2), 1596 (C-C_{Ar}), 1705 (C = O), 1744 (C = O), 2939 (CH_3). ^1H NMR (600 MHz, D_2O): 1.64 (s, 3H), 1.94 (s, 3H), 2.04 (s, 3H), 2.31 (s, 3H), 2.58 (s, 1H), 3.03–3.13 (m, 1H), 3.53–3.60 (m, 1H), 3.85–3.95 (m, 1H), 4.41 (dd, 1H, PCH, $^3J_{\text{HH}}$ 11.74 Hz, $^2J_{\text{PH}}$ 17.08 Hz), 6.19 (s, 1H), 7.36 (d, 1H, $^3J_{\text{HH}}$ 7.71 Hz), 7.72 (t, 1H, $^3J_{\text{HH}}$ 7.56 Hz), 7.85 (t, 1H, $^3J_{\text{HH}}$ 7.55 Hz), 7.99 (d, 1H, $^3J_{\text{HH}}$ 7.69 Hz). ^{13}C NMR (151 MHz, D_2O): 11.0, 18.8, 24.8, 35.7 (d, $^1J_{\text{PC}}$ 229.4 Hz), 49.0 (d, $^2J_{\text{PC}}$ 10.6 Hz), 56.8, 80.1, 118.4 (d, $^2J_{\text{PC}}$ 14.1 Hz), 122.3, 123.4, 125.7, 126.6, 134.0, 137.1, 138.0, 138.4, 141.2, 141.4, 151.1 (d, $^3J_{\text{PC}}$ 6.3 Hz), 201.0, 201.9 (s). ^{31}P NMR (243 MHz, D_2O): 22.7. MS (MALDI TOF), m/z : 434 [M + Na]⁺. Calcd. (%) for $\text{C}_{22}\text{H}_{24}\text{NO}_5\text{P}$: C, 63.92; H, 5.19; O, 20.01 N, 3.39; P, 7.49. Found: C, 64.23; H, 5.39; O, 19.75; N, 3.19; P, 7.43.

(3aS,9bS)-4-hydroxy-7-methoxy-2-methyl-2,3,3a,9b-tetrahydrospiro[benzo [5,6][1,2]oxaphosphinino [3,4-c]pyrrole-1,2'-indene]-1',3'-dione 4-oxide (2b)

Yield 0.36 g (47%), yellow solid, m.p. > 300 °C. IR (ν , cm^{-1}): 1081 (C-O), 1162 (O-CH₃), 1229 (P = O), 1504 (CH_2), 1618 (C-C_{Ar}), 1705 (C = O), 1742 (C = O), 2930 (CH_3). ^1H NMR (600 MHz, D_2O): 2.18 (s, 3H, NCH₃); 3.03–3.12 (m, 1H, CH₂); 3.37–3.44 (mp, 1H, CH); 3.54 (s, 3H, OCH₃); 3.70–3.79 (m, 1H, CH₂) 4.05–4.12 (m, 1H, PCH); 5.97 (d, 1H, CH, $^3J_{\text{HH}}$ 8.19 Hz); 6.17 (d, 1H, CH, $^3J_{\text{HH}}$ 8.43 Hz); 6.44 (s, 1H, CH); 7.34 (d, 1H, CH, $^3J_{\text{HH}}$ 7.54 Hz); 7.73 (t, 1H, CH, $^3J_{\text{HH}}$ 7.15 Hz); 7.85 (t, 1H, CH, $^3J_{\text{HH}}$ 7.49 Hz); 7.96 (d, 1H, CH, $^3J_{\text{HH}}$ 7.57 Hz). ^{13}C NMR (100.6 MHz, D_2O): 35.7 (s); 35.81 (d, $^1J_{\text{PC}}$ 136.4 Hz); 52.0 (d, $^2J_{\text{PC}}$ 4.4 Hz); 56.0 (s); 57.3 (s); 80.8 (s); 106.2 (d, $^2J_{\text{PC}}$ 4.3 Hz); 109.8 (s); 115.2 (s); 115.4 (s); 122.8 (s); 124.1 (s); 130.8 (s); 137.7 (s); 138.4 (s); 142.1 (d, $^3J_{\text{PC}}$ 2.3 Hz); 153.7 (d, $^3J_{\text{PC}}$ 5.9 Hz); 160.2 (s); 202.7 (s); 203.5 (s). ^{31}P NMR (242.9 MHz, D_2O): 21.3. MS (MALDI-TOF) m/z : 420 [M + Na]⁺. Calcd. (%) for $\text{C}_{20}\text{H}_{18}\text{NO}_6\text{P}$: C, 60.15; H, 4.54; O, 24.04; N, 3.51; P, 7.76. Found: C, 60.23; H, 4.39; O, 23.95; N, 3.27; P, 7.52.

(3aS,9bS)-6,8-dichloro-4,9-dihydroxy-2-methyl-2,3,3a,9b-tetrahydrospiro[benzo [5,6][1,2]oxaphosphinino [3,4-c]pyrrole-1,2'-indene]-1',3'-dione 4-oxide (2c)

Yield 0.17 g (25%), yellow solid, m.p. > 300 °C. IR (ν , cm^{-1}): 1078 (C-Cl), 1229 (P = O), 1456 (CH_2), 1591 (C-C_{Ar}), 1703 (C = O), 1736 (C = O), 2871 (CH_3). ^1H NMR (399.93 MHz, D_2O): 2.21 (s, 3H, NCH₃); 3.01–3.15 (m, 1H, CH₂); 3.37–3.44 (m, 1H, CH); 3.64–3.75 (m, 1H, CH₂); 4.36–4.46 (m, 1H, PCH); 7.25 (s, 1H, CH); 7.54 (d, 1H, CH, $^3J_{\text{HH}}$ 7.86 Hz); 7.85 (t, 1H, CH, $^3J_{\text{HH}}$ 7.18 Hz); 7.94 (t, 1H, CH, $^3J_{\text{HH}}$ 7.76 Hz); 8.01 (d, 1H, CH, $^3J_{\text{HH}}$ 7.48 Hz). ^{13}C NMR (100.6 MHz, D_2O): 34.4 (d, $^1J_{\text{PC}}$ 128.6 Hz); 46.5 (s); 56.9 (s); 78.6 (s); 114.6 (d, $^2J_{\text{PC}}$ 15.2 Hz); 115.5 (s); 122.2 (s); 123.4 (s); 129.0 (s); 137.4 (s); 139.9 (s); 142.4 (s); 148.0 (d, $^3J_{\text{PC}}$ 4.9 Hz); 202.2 (s); 203.1 (s). ^{31}P NMR (161.9 MHz, D_2O): 21.2. MS (MALDI-TOF) m/z : 492 [M + K]⁺. Calcd. (%) for $\text{C}_{19}\text{H}_{14}\text{NCl}_2\text{O}_6\text{P}$: C, 50.24; H, 3.11; O, 21.14; Cl, 15.61; N, 3.08; P, 6.82. Found: C, 50.23; H, 3.39; O, 20.95; N, 3.17; P, 6.41.

(3a'S,11a'S)-11'-hydroxy-2'-methyl-1',2',3a',11a'-tetrahydrospiro[indene-2,3'-naphtho [2',1':5,6] oxaphosphinino [3,4-c]pyrrole]-1,3-dione 11'-oxide (2d)

Yield 0.25 g (34.7%), yellow solid, m.p. > 300 °C. IR (ν , cm^{-1}): 1243 (P = O), 1466 (CH_2), 1596 (C-C_{Ar}), 1703 (C = O), 1749 (C = O). ^1H NMR (399.93 MHz, D_2O): 2.25 (s, 3H,

NCH₃); 3.23–3.33 (m, 1H, CH₂); 3.51–3.58 (m, 1H, CH); 3.84–3.96 (m, 1H, CH₂); 4.97 (dd, 1H, PCH, ³J_{HH} 11.87 Hz, ²J_{PH} 16.02 Hz); 7.04–7.09 (m, 2H, CH); 7.13 (t, 1H, CH, ³J_{HH} 7.56 Hz); 7.19 (t, 1H, CH, ³J_{HH} 7.84 Hz); 7.40 (t, 1H, CH, ³J_{HH} 7.62 Hz); 7.42–7.52 (m, 3H, CH); 7.59 (d, 1H, CH, ³J_{HH} 8.87 Hz); 7.64 (d, 1H, CH, ³J_{HH} 7.73 Hz). ¹³C NMR (100.6 MHz, D₂O): 35.6 (d, ¹J_{PC} 136.9 Hz); 47.7 (d, ²J_{PC} 4.35 Hz); 56.7 (s); 80.6 (s); 116.4 (d, ²J_{PC} 15.5 Hz); 120.5 (d, ³J_{PC} 10.1 Hz); 121.3 (d, ³J_{PC} 9.0 Hz); 122.9 (s); 123.3 (s); 124.7 (s); 127.1 (s); 128.6 (s); 130.1 (s); 130.5 (s); 131.5 (s); 136.4 (s); 137.2 (s); 140.2 (s); 141.7 (s); 151.2 (d, ³J_{PC} 6.1 Hz); 202.2 (s); 203.0 (s). ³¹P NMR (161.9 MHz, D₂O): 23.6. MS (MALDI-TOF) *m/z*: 420 [M + 1]⁺, 442 [M + Na]⁺. Calcd: (%) for C₂₃H₁₈NO₅P: C, 65.87; H, 4.33; O, 19.08; N, 3.34; P, 7.39. Found: C, 65.65; H, 4.31; O, 19.01; N, 3.21; P, 7.40.

(6*aS*,6*bR*,11*aS*)-6-hydroxy-1,3,4-trimethyl-6*a*,6*b*,7,8,9,11*a*-hexahydrospiro[benzo [5,6][1,2]oxaphosphinino [3,4-*a*]pyrrolizine-11,2'-indene]-1',3'-dione 6-oxide (**2e**)

Yield 0.28 g (35%), white solid, m.p. > 300 °C. IR (ν, cm⁻¹): 1252 (P = O), 1460 (CH₂), 1591 (C-C_{Ar}), 1708 (C = O), 1751 (C = O), 2929 (CH₃). ¹H NMR (399.93 MHz, D₂O): 1.82 (s, 3H, CH₃); 1.97 (s, 3H, CH₃); 2.01 (s, 3H, CH₃); 2.10–2.29 (m, 2H, CH₂); 2.44–2.57 (m, 2H, CH₂); 2.87–3.00 (m, 1H, CH₂); 3.72–3.80 (m, 1H, CH); 4.23–4.32 (m, 1H, CH₂); 4.95 (dd, 1H, PCH, ³J_{HH} 11.50 Hz, ²J_{PH} 18.93 Hz); 5.51 (s, 1H, CH); 6.26 (s, 1H, CH); 7.49–7.52 (m, 1H, CH); 7.81 (td, 1H, CH, ³J_{HH} 6.35 Hz); 7.87 (td, 1H, CH, ³J_{HH} 7.58 Hz); 8.00–8.04 (m, 1H, CH). ¹³C NMR (100.6 MHz, D₂O): 10.7 (s); 18.4 (s); 18.7 (s); 23.5 (s); 29.5 (d, ³J_{PC} 3.4 Hz) 41.5 (d, ¹J_{PC} 135.1 Hz); 47.1 (d, ²J_{PC} 5.2 Hz); 50.4 (s); 72.0 (s); 77.1 (s); 115.6 (d, ²J_{PC} 14.2 Hz); 122.9 (s); 123.9 (s); 125.9 (d, ³J_{PC} 3.3 Hz); 127.3 (s); 134.3 (s); 137.3 (s); 138.1 (s); 139.5 (s); 139.9 (s); 141.0 (s); 150.5 (d, ³J_{PC} 6.8 Hz); 192.9 (s); 193.8 (s). ³¹P NMR (161.9 MHz, D₂O): 19.0. MS (MALDI-TOF) *m/z*: 460 [M + Na]⁺. Calcd: (%) for C₂₄H₂₄NO₅P: C, 65.90; H, 5.53; O, 18.29; N, 3.20; P, 7.08. Found: C, 65.65; H, 5.31; O, 18.11; N, 3.11; P, 7.00.

(8*a'S*,8*b'R*,13*a'S*)-8'-hydroxy-8*a'*,8*b'*,9',10',11',13*a'*-hexahydrospiro[indene-2,13'-naphtho [2',1':5,6][1,2]oxaphosphinino [3,4-*a*]pyrrolizine]-1,3-dione 8'-oxide (**2f**)

Yield 0.44 g (58%), white solid, m.p. > 300 °C. IR (ν, cm⁻¹): 1223 (P = O), 1465 (CH₂), 1594 (C-C_{Ar}), 1715 (C = O), 1753 (C = O). ¹H NMR (399.93 MHz, CF₃COOD): 2.29–2.41 (m, 1H, CH₂); 2.50–2.62 (m, 1H, CH₂); 2.65–2.73 (m, 1H, CH₂); 2.87–2.96 (m, 1H, CH₂); 3.82–3.92 (m, 1H, CH₂); 3.98–4.09 (m, 1H, CH₂); 4.25–4.35 (m, 1H, CH); 4.39–4.45 (m, 1H, CH); 5.06–5.18 (m, 1H, PCH); 7.39 (d, 1H, CH, ³J_{HH} 8.94 Hz); 7.71–7.82 (m, 2H, CH); 7.86–7.95 (m, 2H, CH); 8.05 (d, 1H, CH, ³J_{HH} 8.97 Hz); 8.11–8.18 (m, 2H, CH); 8.47 (d, 1H, CH, ³J_{HH} 7.31 Hz). ¹³C NMR (100.6 MHz, CF₃COOD): 7.5 (s); 23.2 (s); 25.4 (s); 37.2 (d, ¹J_{PC} 140.9 Hz); 42.9 (s); 51.0 (s); 61.5 (s); 68.5 (d, ³J_{PC} 4.5 Hz); 72.3 (s); 77.4 (d, ²J_{PC} 11.9 Hz); 105.6 (d, ²J_{PC} 11.0 Hz); 115.7 (d, ³J_{PC} 5.7 Hz); 121.0 (s); 121.9 (s); 122.1 (s); 122.2 (s); 123.0 (s); 123.8 (s); 126.1 (s); 126.6 (s); 126.9 (s); 127.4 (s); 127.9 (s); 143.8 (d, ³J_{PC} 6.8 Hz); 147.2 (s); 192.6 (s). ³¹P NMR (161.9 MHz, CF₃COOD): 18.9. MS (ESI) *m/z*: 448 [M + 3]⁺. Calcd: (%) for C₂₅H₂₀NO₅P: C, 67.41; H, 4.53; O, 17.96; N, 3.14; P, 6.95. Found: C, 67.65; H, 4.31; O, 18.01; N, 3.01; P, 6.85.

(8*a'S*,8*b'R*,13*a'S*)-4'-bromo-8'-hydroxy-8*a'*,8*b'*,9',10',11',13*a'*-hexahydrospiro[indene-2,13'-naphtho [2',1':5,6][1,2]oxaphosphinino [3,4-*a*]pyrrolizine]-1,3-dione 8'-oxide (**2g**)

Yield 0.23 g (50%), white solid, m.p. > 300 °C. IR (ν, cm⁻¹): 1085 (C-Br), 1251 (P = O), 1500 (CH₂), 1588 (C-C_{Ar}), 1713 (C = O), 1755 (C = O), 2926 (CH₃). ¹H NMR (399.93 MHz, DMSO-d₆): 1.73–1.84 (m, 1H, CH₂); 1.87–1.94 (m, 1H, CH₂); 2.05–2.16 (m, 2H, CH₂); 2.87–2.97 (m, 2H, CH₂); 3.47–3.55 (m, 1H, CH); 4.75–4.83 (m, 1H, CH); 5.19–5.26 (m, 1H, PCH); 7.09 (d, 1H, CH, ³J_{HH} 8.85 Hz); 7.30–7.36 (m, 2H, CH); 7.43 (d, 1H, CH, ³J_{HH} 9.26 Hz); 7.62 (d, 1H, CH, ³J_{HH} 8.92 Hz); 7.71 (td, 1H, CH, ³J_{HH} 6.55 Hz); 7.71 (td, 1H, CH, ³J_{HH} 8.61 Hz); 7.78 (d, 1H, CH, ³J_{HH} 7.58 Hz); 7.89 (d, 1H, CH, ³J_{HH} 2.1 Hz). ¹³C NMR (100.6 MHz, DMSO-d₆): 24.0 (s); 29.0 (s); 41.4 (d, ¹J_{PC} 131.9 Hz); 45.4 (s); 48.7 (s); 69.9 (s); 77.7 (s); 117.2 (d, ²J_{PC} 14.9 Hz); 117.7 (s); 119.7 (s); 122.5 (d, ³J_{PC} 3.0 Hz); 122.9 (s); 123.7 (s); 125.4 (s); 129.3 (s); 129.6 (s); 130.2 (s); 130.7 (s); 131.5 (s); 136.4 (s); 137.4 (s); 140.1 (s); 141.5 (s); 152.2 (d, ³J_{PC} 6.3 Hz). ³¹P NMR (161.9 MHz, DMSO-d₆): 20.06. MS (ESI) *m/z*: 520 [M-1]. Calcd: (%) for C₂₅H₁₉NBrO₅P: C, 57.27; H, 3.65; O, 15.26; Br, 15.24; N, 2.67; P, 5.91. Found: C, 57.25; H, 3.61; O, 15.01; Br, 15.31; N, 2.61; P, 5.85.

1-methyl-1,3-dihydro-4*H*-spiro[chromeno [4,3-*b*]pyrrole-2,2'-indene]-1',3',4-trione (**4**)

Yield 0.25 g (25%), orange solid, m.p. > 300 °C. IR (ν , cm^{-1}): 1511 (CH_2), 1594 ($\text{C}-\text{C}_{\text{Ar}}$), 1614 ($\text{C}=\text{C}$), 1707 ($\text{C}=\text{O}$), 1750 ($\text{C}=\text{O}$). ^1H NMR (399.93 MHz, CDCl_3): 3.25 (s, 3H, NCH_3); 3.28 (s, 2H, CH_2); 7.24–7.30 (m, 1H, CH); 7.43 (d, 1H, CH, $^3J_{\text{HH}}$ 8.04 Hz); 7.57 (t, 1H, CH, $^3J_{\text{HH}}$ 8.12 Hz); 7.99 (d, 1H, CH, $^3J_{\text{HH}}$ 8.11 Hz); 7.97–8.04 (m, 2H, CH); 8.10–8.15 (m, 2H, CH). ^{13}C NMR (100.6 MHz, CDCl_3): 35.0 (s); 36.2 (s); 78.0 (s); 96.0 (s); 113.2 (s); 118.4 (s); 123.1 (s); 123.4 (s); 124.6 (s); 132.0 (s); 137.1 (s); 141.1 (s); 155.0 (s); 158.1 (s); 159.3 (s); 196.5. MS (ESI) m/z : 330 [M-1]. Calcd: (%) for $\text{C}_{20}\text{H}_{13}\text{NO}_4$: C, 72.50; H, 3.95; O, 19.32; N, 4.23. Found: C, 72.10; H, 3.91; O, 19.31; N, 4.15.

3.3. Biological Studies

3.3.1. Cell Toxicity Assay (MTT-Test)

The toxic effect on cells was determined using the colorimetric method of cell proliferation MTT (Thiazolyl Blue Tetrazolium Bromide, Sigma). For this, 10 μL of MTT reagent in Hank's balanced salt solution (HBSS) (final concentration 0.5 mg/ml) was added to each well. The plates were incubated at 37 °C for 2–3 h in an atmosphere humidified with 5% CO_2 . Absorbance was recorded at 540 nm using an Invitrologic microplate reader (Russia). Experiments for all compounds were repeated three times. The M-HeLa clone 11 human, epithelioid cervical carcinoma, strain of HeLa, clone of M-HeLa; human duodenal cancer cell line (HuTu 80); human breast adenocarcinoma cells (MCF-7) and Chang liver cell line (Human liver cells) from the N. F. Gamaleya Research Center of Epidemiology and Microbiology and the Type Culture Collection of the Institute of Cytology (Russian Academy of Sciences) were used in the experiments. The cells were cultured on a standard nutrient medium "Igla" produced by the Moscow Institute of Poliomyelitis and Viral Encephalitis. M.P. Chumakov by PanEco, with the addition of 10% fetal calf serum and 1% nonessential amino acids (NEAA).

The cells were sown on a 96-well panel from Eppendorf at a concentration of 5×10^3 cells per well with a volume of 100 μL medium, and cultured in a CO_2 incubator at 37 °C. In 48 h after planting the cells, the culture medium was taken into the wells, and 100 μL solutions of the studied drug in the specified dilutions were added to the wells. Dilutions of the compounds were prepared directly in growth medium supplemented with 5% DMSO to improve solubility. The cytotoxic effect of the test compounds was determined at concentrations of 0.1–100 μM . The calculation of the IC_{50} , the concentration of the drug causing inhibition of cell growth by 50%, was performed using the program: MLA—"Quest Graph™ IC_{50} Calculator". AAT Bioquest, Inc., Pleasanton, CA, USA, <https://www.aatbio.com/tools/ic50-calculator> (accessed on 25 January 2022).

3.3.2. Induction of Apoptotic Effects by Test Compounds (Flow Cytometry Assay)

Cell Culture. HuTu 80 cells at 1×10^6 cells/well in a final volume of 2 mL were seeded into six-well plates. After 24 h of incubation, various concentrations of compound **2a** were added to wells.

Cell Apoptosis Analysis. The cells were harvested at 2000 rpm for 5 min and then washed twice with ice-cold PBS, followed by resuspension in binding buffer. Next, the samples were incubated with 5 μL of annexin V- Alexa Fluor 647 (Sigma-Aldrich, St. Louis, MO, USA) and 5 μL of propidium iodide for 15 min at room temperature in the dark. Finally, the cells were analyzed by flow cytometry (Guava easy Cyte, MERCK, Rahway, NJ, USA) within 1 h. The experiments were repeated three times.

3.3.3. Mitochondrial Membrane Potential

Cells were harvested at 2000 rpm for 5 min and then washed twice with ice-cold PBS, followed by resuspension in JC-10 (10 $\mu\text{g}/\text{mL}$) and incubation at 37 °C for 10 min. After the cells were rinsed three times and suspended in PBS, the JC-10 fluorescence was observed by flow cytometry (Guava easy Cyte, MERCK, Rahway, NJ, USA).

3.3.4. Detection of Intracellular ROS

HuTu 80 cells were incubated with compound **2a** at concentrations of IC_{50} for 24 h. ROS generation was investigated using flow cytometry assay and CellROX[®] Deep Red flow cytometry kit. For this HuTu 80 cells were harvested at 2000 rpm for 5 min and then washed twice with ice-cold PBS, followed by resuspension in 0.1 mL of medium without FBS, to which was added 0.2 μ L of CellROX[®] Deep Red and incubated at 37 °C for 30 min. After being washed three times, the cells were suspended in PBS, and the production of ROS in the cells was immediately monitored using a flow cytometer Guava easy Cyte, MERCK, Rahway, NJ, USA).

3.3.5. Statistical Analysis

The IC_{50} values were calculated using the online calculator MLA—Quest Graph[™] IC50 Calculator AAT Bioquest, Inc., Pleasanton, CA, USA, 25 January 2022. The statistical analysis was performed using the Mann-Whitney test ($p < 0.05$). Tabular and graphical data contains averages and standard errors.

4. Conclusions

In conclusion, a series of novel pyrrolidine-fused spiro dihydrophosphacoumarins were obtained via intermolecular [3 + 2] cycloaddition of phosphacoumarins with ninhydrin-based azomethine ylides. The reaction proceeded in a highly regioselective manner, leading to the formation of up to three stereocentres with excellent diastereoselectivity. The mechanism of the reaction was studied with quantum chemistry methods. The obtained results were in a good agreement with the experimental data and indicate that the preferential formation of a single regio- and diastereoisomer is due to kinetic reasons. Additionally, a novel pathway of the reaction of 4-hydroxycoumarin with azomethine ylides has been revealed, which will be a subject for further research. The anti-cancer activities of spiro phosphacoumarins were tested in vitro. The compound possessing three methyl groups in aromatic moiety appeared to be the most potent against all tested cancer cell lines (M-HeLa, HuTu 80 and MCF-7). Its cytotoxicity was up to 2.6-fold higher than the cytotoxicity of a reference compound. At the same time, its cytotoxicity against normal cell lines (Chang liver) was much lower, thus giving the selectivity index ranging from 10 (M-HeLa cell line) to >32 (HuTu 80 cell line). The more detailed studies of the anti-cancer activity of the lead compound revealed that it arrests the cell cycle at the G1/G0 phase and leads to an increased level of ROS in HuTu 80 cells, as well as decreasing the mitochondrial potential. Thus, the death of cancer cells presumably occurs via an intrinsic mitochondrial apoptosis pathway.

Supplementary Materials: The following supporting information can be downloaded at: <https://www.mdpi.com/article/10.3390/ijms232214348/s1>.

Author Contributions: Synthesis—V.V.S., A.V.Z., Y.M.S., E.A.C. and N.O.A.; quantum chemistry studies, writing—review and editing—A.R.K.; writing—original draft preparation, conceptualization—A.S.G.; biological studies—A.P.L. and S.K.A.; biological studies supervision—A.D.V.; X-ray studies—J.K.V.; project administration, supervision—A.R.B. and M.A.P. All authors have read and agreed to the published version of the manuscript.

Funding: Synthetic work: quantum chemistry computations, NMR, MS research and biological studies were conducted by V.V., A.V., Y.M., A.R., A.S., A.D., A.P., S.K., E.A., N.O., A.R. and M.A. at the Arbuzov Institute of Organic and Physical Chemistry, and were funded by the government assignment for the FRC Kazan Scientific Center of RAS. X-ray studies were conducted by J.K. at the N.S. Kurnakov Institute of General and Inorganic Chemistry and were supported by the Ministry of Science and Higher Education of Russia as part of the state assignment of the Kurnakov Institute of General and Inorganic Chemistry of the Russian Academy of Sciences.

Institutional Review Board Statement: Not applicable.

Informed Consent Statement: Not applicable.

Data Availability Statement: The data presented in this study are contained within the article or in Supplementary Materials, or are available upon request from the corresponding authors Ayrat Khamatgalimov or Almir Gazizov.

Acknowledgments: The authors are grateful to the Assigned Spectral-Analytical Center of FRC Kazan Scientific Center of RAS for technical assistance in the research.

Conflicts of Interest: The authors declare no conflict of interest.

References

1. Balewski, L.; Szulta, S.; Jalińska, A.; Kornicka, A. A Mini-Review: Recent Advances in Coumarin-Metal Complexes with Biological Properties. *Front. Chem.* **2021**, *9*, 781779. [[CrossRef](#)] [[PubMed](#)]
2. Srikrishna, D.; Godugu, C.; Dubey, P.K. A Review on Pharmacological Properties of Coumarins. *Mini-Rev. Med. Chem.* **2018**, *18*, 113–141. [[CrossRef](#)]
3. Annunziata, F.; Pinna, C.; Dallavalle, S.; Tamborini, L.; Pinto, A. An Overview of Coumarin as a Versatile and Readily Accessible Scaffold with Broad-Ranging Biological Activities. *Int. J. Mol. Sci.* **2020**, *21*, 4618. [[CrossRef](#)] [[PubMed](#)]
4. Kaur, M.; Kohli, S.; Sandhu, S.; Bansal, Y.; Bansal, G. Coumarin: A Promising Scaffold for Anticancer Agents. *Anticancer. Agents Med. Chem.* **2015**, *15*, 1032–1048. [[CrossRef](#)]
5. Thakur, A.; Singla, R.; Jaitak, V. Coumarins as anticancer agents: A review on synthetic strategies, mechanism of action and SAR studies. *Eur. J. Med. Chem.* **2015**, *101*, 476–495. [[CrossRef](#)] [[PubMed](#)]
6. Wu, Y.; Xu, J.; Liu, Y.; Zeng, Y.; Wu, G. A Review on Anti-Tumor Mechanisms of Coumarins. *Front. Oncol.* **2020**, *10*, 592853. [[CrossRef](#)] [[PubMed](#)]
7. Rawat, A.; Vijaya Bhaskar Reddy, A. Recent advances on anticancer activity of coumarin derivatives. *Eur. J. Med. Chem. Reports* **2022**, *5*, 100038. [[CrossRef](#)]
8. Li, X.; Zhang, D.; Pang, H.; Shen, F.; Fu, H.; Jiang, Y.; Zhao, Y. Synthesis of a Diverse Series of Phosphacoumarins with Biological Activity. *Org. Lett.* **2005**, *7*, 4919–4922. [[CrossRef](#)]
9. Alexieva, V.; Karanov, E.; Nikolova, R.; Bojilova, A. Plant growth regulating activity of some phosphorus derivatives of coumarin. *Bulg. J. Plant Physiol.* **1995**, *21*, 45.
10. Kim, C.-E.; Ryu, T.; Kim, S.; Lee, K.; Lee, C.-H.; Lee, P.H. Gold-Catalyzed Hydroarylation of Aryl Alkynylphosphonates for the Synthesis of Phosphacoumarins. *Adv. Synth. Catal.* **2013**, *355*, 2873–2883. [[CrossRef](#)]
11. Hariri, M.; Darvish, F.; Mengue Me Ndong, K.-P.; Sechet, N.; Chacktas, G.; Boosaliki, H.; Tran Do, M.L.; Mwande-Maguene, G.; Lebibi, J.; Burirov, A.R.; et al. Gold-Catalyzed Access to Isophosphinoline 2-Oxides. *J. Org. Chem.* **2021**, *86*, 7813–7824. [[CrossRef](#)] [[PubMed](#)]
12. Hariri, M.; Darvish, F.; Ndong, K.-P.M.M.; Babouri, R.; Babouri, R.; Mwande-Maguene, G.; Burirov, A.R.; Licznar-Fajardo, P.; Pirat, J.-L.; Ayad, T.; et al. Biologically relevant surrogates of coumarins: 2-phenyl H-isophosphinoline 2-oxides with antibacterial activity. *GSC Biol. Pharm. Sci.* **2021**, *16*, 283–296. [[CrossRef](#)]
13. Balašova, A.; Žalubovskis, R. Synthetic Methods toward Phosphacoumarins (microreview). *Chem. Heterocycl. Compd.* **2022**, *58*, 310–312. [[CrossRef](#)]
14. Koleva, A.I.; Petkova-Yankova, N.I.; Nikolova, R.D. Synthesis and Chemical Properties of 3-Phosphono-coumarins and 1,2-Benzoxaphosphorins as Precursors for Bioactive Compounds. *Molecules* **2019**, *24*, 2030. [[CrossRef](#)] [[PubMed](#)]
15. Huang, T.; Wang, Q.; Kong, D.; Wu, M. Diastereoselective catalyst-free construction of isoxazolidine-cis-fused phosphadihydrocoumarins via an intramolecular Nitron–Vinylphosphonate dipolar cycloaddition. *Tetrahedron Lett.* **2019**, *60*, 150913. [[CrossRef](#)]
16. Jiang, J.; Wu, M.; Zhu, Z.; Kong, D. Catalyst-Free Intramolecular 1,3-Dipolar Cycloaddition of Ethyl (2-Formylphenyl) Vinylphosphonates: A Highly Stereoselective Access to Phosphadihydrocoumarin-Fused Pyrrolizidines/Pyrrolidines. *Synthesis* **2017**, *49*, 3731–3739. [[CrossRef](#)]
17. Wu, M.; Jiang, J.; Zhu, Z.; Wang, Q.; Kong, D. One-Pot Catalyst-Free Domino Condensation/Intramolecular 1,3-Dipolar Cycloaddition: Highly Stereoselective Access to Phosphadihydrocoumarin-Fused N,N-Bicyclic Pyrazolidin-3-ones. *Synthesis* **2018**, *50*, 139–145. [[CrossRef](#)]
18. Petkova, N.I.; Nikolova, R.D.; Bojilova, A.G.; Rodios, N.A.; Kopf, J. Synthesis of heterocyclic methylenebisphosphonates by 1,3-dipolar cycloaddition of ethyl diazoacetate to 1,2-benzoxaphosphorin-3-phosphonates. *Tetrahedron* **2009**, *65*, 1639–1647. [[CrossRef](#)]
19. Huang, T.; Liu, L.; Wang, Q.; Wu, M.; Kong, D. 1,3-Dipolar Cycloaddition of 3-Amino Oxindole-Based Azomethine Ylides and O-Vinylphosphonylated Salicylaldehydes for Diastereoselective Synthesis of Oxindole Spiro-P,N-polycyclic Heterocycles. *Synthesis* **2020**, *52*, 1387–1397. [[CrossRef](#)]
20. Li, D.-F.; Gu, Y.; Zhang, J.-R.; Liu, K.; Zhao, L.-M. Diastereoselective Construction of Spiro-furo[3,2-c]benzopyranoxindoles through a Cu(OTf)₂/AcOH Cooperative Promoted Bicyclization Reaction. *J. Org. Chem.* **2019**, *84*, 879–887. [[CrossRef](#)]
21. Kowalczyk-Dworak, D.; Albrecht, Ł. α,β -Unsaturated butenolides in an organocatalytic doubly annulative cascade for the preparation of 3,4-dihydrocoumarins. *Org. Biomol. Chem.* **2019**, *17*, 2624–2628. [[CrossRef](#)]

22. Ming, Y.-C.; Lv, X.-J.; Liu, M.; Liu, Y.-K. Synthesis of Chiral Polycyclic Tetrahydrocarbazoles by Enantioselective Aminocatalytic Double Activation of 2-Hydroxycinnamaldehydes with Dienals. *Org. Lett.* **2021**, *23*, 6515–6519. [CrossRef]
23. Hussain, M.; Niu, C.; Wang, G.-W. Palladium-catalyzed synthesis of [60]fullerene-fused furochromenones and further electrochemical functionalization. *Org. Chem. Front.* **2020**, *7*, 1249–1254. [CrossRef]
24. Sadykova, Y.M.; Sadikova, L.M.; Zalaltdinova, A.V.; Sultanova, Z.N.; Burirov, A.R.; Pudovik, M.A. 2H-Benzo[e]-1,2-oxaphosphorine Related Heterocycles as Precursors for the Synthesis of Unsymmetrical Bicyclic Phosphonates. *Russ. J. Gen. Chem.* **2018**, *88*, 1941–1943. [CrossRef]
25. Sadykova, Y.M.; Zalaltdinova, A.V.; Smailov, A.K.; Trofimova, L.M.; Voronina, J.K.; Burirov, A.R.; Pudovik, M.A. Synthesis of unsymmetrical cage phosphonates from heterocyclic systems based on 2H-1,2-benzoxaphosphinine. *Chem. Heterocycl. Compd.* **2020**, *56*, 1605–1610. [CrossRef]
26. Zalaltdinova, A.V.; Sadykova, Y.M.; Smailov, A.K.; Trofimova, L.M.; Burirov, A.R.; Pudovik, M.A. New intramolecular cyclization of 2 H-benzo[e]-1,2-oxaphosphorine derivatives—A way to the synthesis of unsymmetrical cage phosphonates. *Phosphorus. Sulfur. Silicon Relat. Elem.* **2022**, *197*, 549–550. [CrossRef]
27. Das, S. Recent applications of ninhydrin in multicomponent reactions. *RSC Adv.* **2020**, *10*, 18875–18906. [CrossRef] [PubMed]
28. Filatov, A.S.; Wang, S.; Khoroshilova, O.V.; Lozovskiy, S.V.; Larina, A.G.; Boitsov, V.M.; Stepanov, A.V. Stereo- and Regioselective 1,3-Dipolar Cycloaddition of the Stable Ninhydrin-Derived Azomethine Ylide to Cyclopropenes: Trapping of Unstable Cyclopropene Dipolarophiles. *J. Org. Chem.* **2019**, *84*, 7017–7036. [CrossRef]
29. Peña-Morán, O.; Villarreal, M.; Álvarez-Berber, L.; Meneses-Acosta, A.; Rodríguez-López, V. Cytotoxicity, Post-Treatment Recovery, and Selectivity Analysis of Naturally Occurring Podophyllotoxins from *Bursera fagaroides* var. *fagaroides* on Breast Cancer Cell Lines. *Molecules* **2016**, *21*, 1013. [CrossRef]
30. Becke, A.D. Density-functional thermochemistry. III. The role of exact exchange. *J. Chem. Phys.* **1993**, *98*, 5648–5652. [CrossRef]
31. Lee, C.; Yang, W.; Parr, R.G. Development of the Colle-Salvetti correlation-energy formula into a functional of the electron density. *Phys. Rev. B* **1988**, *37*, 785–789. [CrossRef] [PubMed]
32. Hehre, W.J.; Ditchfield, R.; Pople, J.A. Self-Consistent Molecular Orbital Methods. XII. Further Extensions of Gaussian-Type Basis Sets for Use in Molecular Orbital Studies of Organic Molecules. *J. Chem. Phys.* **1972**, *56*, 2257–2261. [CrossRef]
33. Ditchfield, R.; Hehre, W.J.; Pople, J.A. Self-Consistent Molecular-Orbital Methods. IX. An Extended Gaussian-Type Basis for Molecular-Orbital Studies of Organic Molecules. *J. Chem. Phys.* **1971**, *54*, 724–728. [CrossRef]
34. Petersson, G.A.; Bennett, A.; Tensfeldt, T.G.; Al-Laham, M.A.; Shirley, W.A.; Mantzaris, J. A complete basis set model chemistry. I. The total energies of closed-shell atoms and hydrides of the first-row elements. *J. Chem. Phys.* **1988**, *89*, 2193–2218. [CrossRef]
35. Frisch, M.J.; Trucks, G.W.; Schlegel, H.B.; Scuseria, G.E.; Robb, M.A.; Cheeseman, J.R.; Scalmani, G.; Barone, V.; Petersson, G.A.; Nakatsuji, H.; et al. *Gaussian 16; Revision B.01*; Gaussian Inc.: Wallingford, CT, USA, 2016.
36. Bursch, M.; Mewes, J.-M.; Hansen, A.; Grimme, S. Best-Practice DFT Protocols for Basic Molecular Computational Chemistry. *Angew. Chem. Int. Ed.* **2022**, *61*, e202205735. [CrossRef]
37. Zhao, Y.; Truhlar, D.G. Design of Density Functionals That Are Broadly Accurate for Thermochemistry, Thermochemical Kinetics, and Nonbonded Interactions. *J. Phys. Chem. A* **2005**, *109*, 5656. [CrossRef]
38. Rappoport, D.; Furche, F. Property-optimized Gaussian basis sets for molecular response calculations. *J. Chem. Phys.* **2010**, *133*, 134105. [CrossRef]
39. Li, Y. Energy Diagram Plotter (CDXML). Available online: https://github.com/liyuanhe211/Energy_Diagram_Plotter_CDXML (accessed on 10 September 2022).
40. Sheldrick, G.M. *SADABS, Program for Empirical Absorption Correction of Area Detector Data*; University of Gottingen: Gottingen, Germany, 1997.
41. Sheldrick, G.M. SHELXT—Integrated space-group and crystal-structure determination. *Acta Crystallogr. Sect. A Found. Adv.* **2015**, *71*, 3. [CrossRef]
42. Dolomanov, O.V.; Bourhis, L.J.; Gildea, R.J.; Howard, J.A.K.; Puschmann, H. OLEX2: A complete structure solution, refinement and analysis program. *J. Appl. Crystallogr.* **2009**, *42*, 339–341. [CrossRef]
43. Sadykova, Y.M.; Sadikova, L.M.; Badrtdinova, A.R.; Dobrynin, A.B.; Burirov, A.R.; Pudovik, M.A. Condensation of 2-Ethoxyvinylphosphonic Acid Dichloroanhydride with 2,3,5-Trimethylphenol. Novel Method for Preparation of Phosphacoumarins. *Phosphorus. Sulfur. Silicon Relat. Elem.* **2015**, *190*, 2267–2272. [CrossRef]